Rotational invariance and magnetoelastic phenomena in paramagnets*

P. S. Wang and B. Lüthi†
Physics Department, Rutgers University, New Brunswick, New Jersey 08903
(Received 1 November 1976)

We measured sound-velocity changes for various geometries in the model paramagnet TmSb and in high magnetic fields. By measuring the c_{44} mode with propagation direction $\vec{k}$ parallel and perpendicular to the magnetic field one finds a field-dependent splitting between the two modes, which should be absent in noninvariant magnetoelastic theory. This is evidence for the presence of rotationally invariant magnetoelastic interactions. A recently developed theory by Dohm and Fulde is used to quantitatively account for this effect. All relevant material parameters are known for TmSb and we can therefore make for the first time a test for this theory without adjustable parameters. The result is a surprisingly good agreement between experiment and theory. The inclusion of other higher-order magnetoelastic terms is discussed. A similar effect is observed for the c_{11}-c_{12} mode, where we can account for the mode splitting with opposite sign to the c_{44} case and where we can account for the order of magnitude of the effect with a simplified calculation. We also present analogous experimental results for paramagnetic Pr_3Te_4 in smaller fields, which we do not interpret quantitatively due to lack of knowledge of crystal electric field parameters for Pr^{3+}.

I. INTRODUCTION

We present experimental results of sound-velocity measurements in high magnetic fields for various paramagnetic substances and for special elastic propagation modes. These experiments allow us to make a quantitative test of rotationally invariant magnetoelastic theories. We give results for the model substance TmSb for which all relevant parameters are known. Therefore, we can make a quantitative comparison between theory and experiment for this compound without any adjustable parameters. This results, therefore, in the first truly quantitative test for rotationally invariant theories. The result is a good agreement between theory and experiment. It also constitutes the first such experiment for cubic materials.

In the noninvariant magnetoelastic theory[1] one has a linear coupling between the symmetric strain and the quadrupole operators of the magnetic ion. This theory successfully explains magnetostriction experiments for various materials[1,2] and also the temperature dependence of elastic constants in the paramagnetic phase for many rare-earth compounds.[3,4]

However, it was noted by various people that such a magnetoelastic theory violates the principle of rotational invariance.[5-7] That is to say that the magnetoelastic Hamiltonian used to describe experiments such as the ones mentioned above does not exhibit rotational invariance. Rotationally invariant magnetoelastic theories were experimentally tested for the first time by Melcher[8] for MnF_2 in the antiferromagnetic state. He showed that, due to rotational deformation the c_{44} mode measured with respect to different magnetic-field directions exhibited different field behavior. More recently similar results were found in the paramagnetic phase of rare-earth vanadates.[9] In all these experimental tests the magnetoelastic coupling constants and crystal-field parameters were not known, in fact certain linear combinations of them were determined from these experiments. As mentioned above, in certain cubic rare-earth compounds all these parameters are known from other experiments. Therefore, with the help of a recently developed theory of rotationally invariant magnetoelastic interaction in rare-earth paramagnets,[10] we can make a quantitative test of these phenomena. A brief account of part of this work was given at a recent conference.[11]

In Sec. II we describe experimental details. In Sec. III we give an elementary account of the rotational invariant theories and derive all necessary formulas. In Sec. IV we give the experimental results and discuss them in great detail.

II. EXPERIMENT

The bulk of the experimental results will be concerned with TmSb. However, we also give results for Pr_3Te_4 and we mention $Pr_{0.05}La_{0.95}Al_2$. Since we know all relevant parameters only for TmSb, we shall give only a quantitative discussion for this compound. Many of the relevant facts for these materials have been discussed previously: TmSb,[3,4] Pr_3Te_4.[12]

Single crystals of TmSb were grown by Bucher by direct fusion and subsequent solidification in a sealed tantalum crucible over a large temperature gradient. This produced crystallites of varying sizes, depending on the particular rare-earth compounds. Single crystals were cut out with a

spark cutter and oriented using an x-ray goniometer. The growth of single crystals of Pr_3Te_4 is described elsewhere.[13]

We investigated three crystals of TmSb and one crystal of Pr_3Te_4. Two of the TmSb crystals, which were used for the c_{44} mode were cut with end faces normal to the three cubic axis. The dimensions of these crystals were $2.49\times2.45\times2.20$ mm^3 [TmSb (1)] and $1.5\times2.6\times4.95$ mm^3 [TmSb (2)], e.g., two sides were of the same length for TmSb (1) enabling us to have the same geometry with respect to an applied magnetic field along the two sides. The third TmSb crystal [TmSb (3)], which was used for the c_{11}-c_{12} mode, was the one used in the previous investigation[3] and had dimensions of 3.24 mm along the [110] axis, 3.14 mm along the [001], and 2.9 mm along the $[1\bar{1}0]$ axis. Finally, for Pr_3Te_4 the cubic side lengths were $3.80\times3.82\times3.70$ mm^3.

We used a high-resolution phase comparison method to measure sound velocity,[14] (1 part in 10^6 resolution) which was used in previous investigations. The thermal expansion[15] and magnetostriction[16] of the TmSb sample were known and we will discuss these corrections in Sec. IV.

A superconducting magnet capable of attaining 90 kOe was used for these measurements. We constructed a sample holder to measure sound-velocity changes for propagation either parallel or perpendicular to the magnetic field. For the temperature measurements we used a capacitive thermometer (Lake Shore Cryotronics) and a calibrated germanium thermometer. Most of the measurements were performed at 2 K with some at 4 K and higher. However, we only calculated sound-velocity changes theoretically for low temperatures and we therefore compare only the 2-K data with theory.

III. THEORY

We give here a simple derivation of the rotationally invariant magnetoelastic interaction and of the corresponding sound-velocity expressions. A detailed theory, applicable to the case of cubic rare-earth compounds, can be found in Ref. 10. The starting point is the crystal field (CEF) and magnetoelastic strain (str) Hamiltonian $\mathcal{H}=\mathcal{H}_{\rm CEF}+\mathcal{H}_{\rm str}$ which are, for cubic symmetry and for c_{44} and c_{11}-c_{12} modes,[17]

$$\mathcal{H}_{\rm CEF}=B_4(O_4^0+5O_4^4)+B_6(O_6^0-21O_6^4),$$
$$\mathcal{H}_{\rm str}=\tfrac{1}{6}G_2(2E_{zz}-E_{xx}-E_{yy})O_2^0+\tfrac{1}{2}G_2(E_{xx}-E_{yy})O_2^2+G_3E_{xy}(J_xJ_y+J_yJ_x)+\cdots. \quad (1)$$

In Eq. (1), the O_4, O_6, O_2^2, J_xJ_y are the well-known crystal field and quadrupole operators,[18] $E_{ij}=\frac{1}{2}(v_{ij}+v_{ji}+\sum_\gamma v_{\gamma i}v_{\gamma j})$ is the component of the finite strain tensor, and v_{ij} is the component of the deformation tensor. $\epsilon_{ij}=\frac{1}{2}(v_{ij}+v_{ji})$, $\omega_{ij}=\frac{1}{2}(v_{ij}-v_{ji})$ are the infinitesimal strain and rotation tensor components. With the help of Eq. (1) we could successfully account for the temperature dependence of the various elastic constants in many rare-earth compounds.[3,4,12] However, in order to understand the magnetic field dependence of some symmetry-elastic constants one has to introduce a rotationally invariant magnetoelastic Hamiltonian. For example, Eq. (1) predicts the same magnetic field dependence of the c_{44} mode for sound waves propagating parallel to the field and perpendicular to the field, whereas the correct magnetoelastic Hamiltonian will give different magnetic field behavior for the two modes in agreement with experiment.

Rotational invariance requires the interaction of a magnetic ion, characterized by $\vec{J}_n$, with the strained and rotated lattice to be equal to the interaction of the reversely rotated spin $\underline{R}_{\rm rot}^{-1}\vec{J}_n$ with the purely strained lattice[10]: If one writes a general deformation of a lattice point $\vec{R}_n$ as a product of a pure strain deformation and a rotation $\underline{R}_{\rm rot}^{10}$, e.g., $(1+\underline{v}_n)\vec{R}_n=\underline{R}_{\rm rot}(1+2\underline{E}_n)^{1/2}\vec{R}_n$ then rotational invariance means

$$\mathcal{H}(\vec{J}_n,(1+\underline{v}_n)\vec{R}_n)=\mathcal{H}(\vec{J}_n,\underline{R}_{\rm rot}(1+2\underline{E}_n)^{1/2}\vec{R}_n)=\mathcal{H}(\underline{R}_{\rm rot}^{-1}\vec{J}_n;(1+2\underline{E}_n)^{1/2}\vec{R}_n). \quad (2)$$

We apply this principle to the special case of sound propagation in the x-z plane which is realized experimentally in our experiment. In this case we can choose the finite rotation tensor as

$$\underline{R}_{\rm rot}=\begin{pmatrix}1-\frac{1}{2}\omega_{xz}^2 & 0 & \omega_{xz}\\ 0 & 1 & 0\\ -\omega_{xz} & 0 & 1-\frac{1}{2}\omega_{xz}^2\end{pmatrix}$$

and operate it on Eq. (1). To second order in ω_{xz}, $\underline{R}_{\rm rot}$ describes a rotation about y axis with angle ω_{xz}. In this way the CEF term $B_4O_4=-20B_4(J_x^2J_z^2+J_z^2J_x^2)$ transforms into $-20B_4\omega_{xz}\Lambda_{xz}+40B_4\omega_{xz}^2\lambda_{xz}$, where $\Lambda_{xz}=(J_x^2-J_z^2)(J_xJ_z+J_zJ_x)+(J_xJ_z+J_zJ_x)(J_x^2-J_z^2)$ and $\lambda_{xz}=(J_xJ_z+J_zJ_x)^2-(J_x^2-J_z^2)^2$. Furthermore the strain term $G_3\epsilon_{xz}(J_xJ_z+J_zJ_x)$ transforms into $2G_3\epsilon_{xz}\omega_{xz}(J_x^2-J_z^2)$. For the c_{44} mode the rotational part of the magnetoelastic Hamiltonian therefore reads

$$\mathcal{H}_{\rm rot}(c_{44})=-20B_4\omega_{xz}\Lambda_{xz}+40B_4\omega_{xz}^2\lambda_{xz}+2G_3\epsilon_{xz}\omega_{xz}(J_x^2-J_z^2). \quad (3)$$

This result agrees with the result of a derivation using general relations between tensor operators.[10]

In Eq. (3) we used only the infinitesimal strain tensor components ϵ_{xz}, ω_{xz}. The finite strain tensor E_{ij} in Eq. (2) also gives for the c_{44} mode contributions involving E_{xx}, E_{zz} which leads to the following second-order Hamiltonian[19]:

$$\mathcal{H}^{(2)} = G_2(J_z^2 - J_x^2)\epsilon_{xz}\omega_{xz} + \tfrac{1}{2}G_2(J_x^2 + J_z^2)(\epsilon_{xz}^2 + \omega_{xz}^2). \tag{4}$$

The contributions of this term we shall discuss separately.

In an analogous way we derive $\mathcal{H}_{\rm rot}$ for the c_{11}-c_{12} mode[19]:

$$\mathcal{H}_{\rm rot}(c_{11}-c_{12}) = -20B_4\omega_{xy}\Lambda_{xy} + 40B_4\omega_{xy}^2\lambda_{xy} - 2G_2(J_xJ_y + J_yJ_x)\epsilon_{xx}\omega_{xy}. \tag{5}$$

In order to calculate the elastic constants we use the same thermodynamic formulation as before[3,4] except that instead of defining the isothermal elastic constants as $c_\Gamma = (\partial^2 F/\partial\epsilon_\Gamma^2)_T$, we now use for the c_{44} modes

$$\Delta c_{xz} = \left(\frac{\partial^2 F}{\partial v_{xz}^2}\right)_T, \quad \Delta c_{zx} = \left(\frac{\partial^2 F}{\partial v_{zx}^2}\right)_T. \tag{6}$$

Here Δc_{xz} means the elastic constant contribution due to a v_{xz} deformation (propagation vector k_z, polarization vector R_x). Previous workers have shown pictorially how in a v_{xz} and a v_{zx} deformation of a plane wave the rotational contributions ω_{xz} and ω_{zx} act in the opposite sense,[4,9,10] therefore giving rise to measurable differences in the presence of a magnetic field. Furthermore, in Fig. 1 of Ref. 9 it is clearly shown how the finite strain term contributions E_{xx} and E_{zz} arise which are responsible for $\mathcal{H}^{(2)}$ [Eq. (4)].

With $\mathcal{H}_{\rm CEF}$, $\mathcal{H}_{\rm str}$ and $\mathcal{H}_{\rm rot}$ [Eqs. (1) and (3)], and the Zeeman term $\mathcal{H}_z = -g\mu_B J_z H_z$ one can calculate the dependence of the crystal-field energy levels $E(\Gamma_n)$ on H, ϵ_{xz}, ω_{xz}: $E(\Gamma_n, H, \epsilon_{xz}, \omega_{xz})$. From this, one can calculate the free-energy density $F = -kTN\ln\sum_n \exp(-E_n/kT)$ and with Eq. (6) Δc_{ij}. The result, in agreement with the Green's-function treatment[10] gives for the c_{44} mode

$$\begin{aligned}(k_z, R_x)\Delta v_{xz}/v_0 &= (N/2\rho v_0^2)\{\tfrac{1}{4}\chi[G_3(J_xJ_z + J_zJ_x) - 20B_4\Lambda_{xz}] + 20B_4\langle\lambda_{xz}\rangle + G_3\langle J_x^2 - J_z^2\rangle\},\\ (k_x, R_z)\Delta v_{zx}/v_0 &= (N/2\rho v_0^2)\{\tfrac{1}{4}\chi[G_3(J_xJ_z + J_zJ_x) + 20B_4\Lambda_{xz}] + 20B_4\langle\lambda_{xz}\rangle - G_3\langle J_x^2 - J_z^2\rangle\}.\end{aligned} \tag{7}$$

Here χ is the strain susceptibility defined previously.[3,4,10] It arises from the terms linear in $\omega_{xz}, \epsilon_{xz}$ of Eqs. (1) and (3). Terms quadratic in $\epsilon_{xz}, \omega_{xz}$ give the thermal-averaged contributions $\langle\ \rangle$. v_0 is the $H = 0$ background sound velocity and Δv the change in the field. ρ is the density and N the number of molecules per unit volume.

In the Appendix we give details of the actual numerical calculation for the c_{44} in TmSb. Various approximations in the theory and calculations (such as the neglect of B_6 in $\mathcal{H}_{\rm rot}$) will be discussed in Sec. IV.

IV. RESULTS AND DISCUSSION

A. TmSb: Material constants

TmSb is a paramagnet which does not exhibit any magnetic or structural phase transition. It has the following further attractive features: It has a cubic NaCl structure. The Tm ion is in a definite Tm^{3+} ($J = 6$) valence state. Exchange between ions is negligible. This was deduced from susceptibility measurements[20] in the system $Tm_x Y_{1-x}$ Sb. This result was confirmed by inelastic neutron scattering experiments.[21] These experiments also gave CEF parameters $B_4 = 13 \pm 0.2$ mK, $B_6 = 0.0286 \pm 0.0026$ mK, therefore, the wave functions are known[22] (see the Appendix). It is seen that B_6 is much smaller than B_4. This permits us to neglect B_6 terms compared to B_4 terms in our analysis of Eq. (3), etc., as has been done in Sec. III and in the literature.[10] This is justified although the matrix elements for O_6 operators are substantially larger than for O_4 operators. An estimate for a typical matrix element gives[18] $B_6\langle 6|O_6^0|6\rangle / B_4\langle 6|O_4^0|6\rangle = 0.06$. Therefore we expect to make at most a 10% error in neglecting B_6 terms. For our numerical calculation we take $B_4 = 13$ mK.

The values of B_4, B_6 lead to the following level scheme (number in parentheses in degrees Kelvin) $\Gamma_1 - \Gamma_4(25) - \Gamma_5^2(56) - \Gamma_2(115) - \Gamma_5^1(187) - \Gamma_3(200)$. At 2 K the thermal population of the excited levels is smaller than 10^{-5} and therefore negligible. One has only to consider matrix elements out of the ground state. In the Appendix we have listed matrix elements for a number of magnetic field values.

The magnetoelastic coupling constants we determine from the fit to the temperature dependence of the c_{44} and c_{11}-c_{12} modes.[3,4] In Fig. 1 we show the temperature dependence of c_{44} for two of our samples: TmSb (3) was the one we investigated previously and TmSb (1) is the one which was used to measure the rotational contributions to c_{44} discussed below. It is seen from Fig. 1 that the elastic constants of the two samples exhibit the minimum both at 9 K, however, the sample

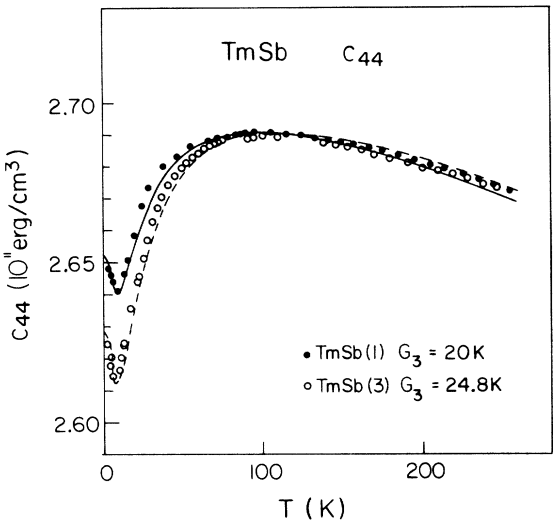

FIG. 1. Temperature dependence of elastic constants c_{44} in TmSb for two samples TmSb (1) and (2) (full circles) and TmSb (3) (open circles). Lines are fitted strain susceptibilities.

TmSb (1) exhibits a smaller minimum leading to a magnetoelastic coupling constant G_3 20% lower than the one for TmSb (3). Such a variation of magnetoelastic coupling constants is found very often in these rare-earth compounds.[4] It is related to similar variations in transition temperatures and is due to slight differences in stochiometry, impurities, etc. For our purpose it is therefore important to use the coupling constants measured on the actual sample, because the rotational effects are a sensitive function of G_3. For our analysis below we use for $G_3 = 20$ K for the c_{44} mode. The elastic measurements give only $|G_3|$. The sign of G_3 we took from the point-charge model (PCM), because the sign and magnitude of G_2 as determined from magnetostriction agrees very well with PCM for the whole LSb series.[16]

B. TmSb: Rotational effects for the c_{44} mode

In Fig. 2 we show relative velocity changes $\Delta v/v_0$ for sample TmSb (1) for the c_{44} mode in the two geometries k_z, R_x and k_x, R_z. TmSb (1) and TmSb (2) gave the same result within 10%. For the zero-field velocity we take $v_0 = 1.77$ km/sec $\rho = 8.57$ g/cm^3. One notes a clear effect of rotational contribution: at 60 kOe there is 0.5% difference between the modes which would be degenerate in noninvariant magnetoelastic theory.

We first discuss possible experimental corrections:

(i) Magnetostriction correction. The magnetostriction along [100] direction at 2 K in TmSb is[16] $\delta l/l = 10^{-5}$ for $H = 15$ kOe. With an H^2 extrapolation

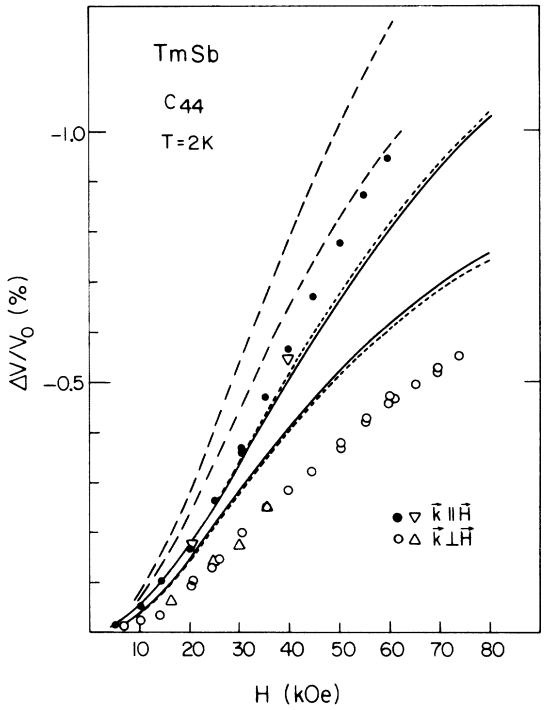

FIG. 2. Relative velocity change in large magnetic fields for c_{44} mode in TmSb at $T = 2$ K, full circle is mode $\vec{k} \parallel \vec{H}$ polarization vector $\vec{R} \perp \vec{H}$, open circle $\vec{k} \perp \vec{H}$, $\vec{R} \parallel \vec{H}$. Dashed-line calculation [Eq. (7)] using $G_3 = 24.8$ K, solid-line calculation using $G_3 = 20$ K, dotted-line calculation Eq. (7) with $\mathcal{H}^{(2)}$ contributions included. Δ, ∇, 30 MHz.

as an upper limit, we get 1.6×10^{-4} for 60 kOe. This gives in the scale of Fig. 2 a change of 0.016% for $\Delta v/v_0$ at the highest field which is practically negligible. Because of the same side lengths, the same magnetostriction correction applies for both modes, for TmSb (1).

(ii) Demagnetizing field: The magnetic susceptibility at 2 K is $\chi = 0.505$ cm^3/mol which gives an upper limit for $M = 14.8H \times 10^{-3}$ G. For the TmSb (1) sample we get as demagnetizing coefficients in the field direction for an inscribed ellipsoid $N = 4$ which leads to an upper limit of the demagnetizing field of 3.5 kG at 60 kOe, which again does not give an important correction.

(iii) Since this demagnetizing field is so small, we can neglect its variation along the axis of the specimen due to the nonellipsoidal form of the specimen.

With all these experimental corrections considered, we can compare our experimental results with the theoretical calculations. In Fig. 2, we have plotted theoretical curves, calculated on the basis of Eq. (7). The material constants used were discussed in Sec. IV A. The full line is with the magnetoelastic coupling constant deduced

from Fig. 1 for the sample TmSb (1) ($G_3 = 20$ K), the dashed line with G_3 from the previous sample TmSb (3) ($G_3 = 24.8$ K). It is seen that the theoretical curves depend sensitively on G_3. Details of the calculation are given in the Appendix. It is rather amazing that the best choice of B_4 and G_3 gives a surprisingly good fit to the experiment, the deviation being only about 20% for both modes. In Ref. 11 we performed a similar calculation including only the lowest 3 levels $\Gamma_1\Gamma_4\Gamma_5^2$. This leads to small differences as a comparison of Table I rows 7, 8 and 9, 10 show. We now discuss possible additional contributions:

(i) Inclusions of terms due to the sixth-order CEF parameter B_6. This we believe is the most serious omission in the theory. In Sec. IV A we estimated a typical matrix element and found that it could account for up to 6% of the corresponding B_4 matrix element. However, the calculational effort involved in including these terms is very large.

(ii) One has to consider higher-order contributions to the theory as discussed in Sec. III. We have considered the second-order Hamiltonian $\mathcal{H}^{(2)}$ arising from the finite strain tensor contributions [Eq. (4)]. With $G_2 = -63$ K this gives an almost negligible contribution as can be seen from Table I, rows 11 and 12, where we have listed it for various field values. The largest contribution for 80 kG is -3.6×10^{-4} for $(\Delta v_{xz} - \Delta v_{zx})/v_0$, its contribution is given by the dotted line in Fig. 2.

(iii) Another second-order strain contribution comes from higher-order magnetoelastic coupling constants[19]:

$$\mathcal{H}^{(3)} = fE_{xz}^2\left[J_x^2 + J_z^2 - \tfrac{3}{5}(J_x^2J_z^2 + J_z^2J_x^2) + \tfrac{1}{5}(J_x^4 + J_z^4) - \tfrac{3}{5}J(J+1)\right],$$

where one can estimate f from a PCM calculation. Since such estimates give f an order of magnitude smaller than G_3 and since the expectation values of the operators change little with field, these terms can also be neglected.[19] In any case these terms do not contribute to the splitting of the two modes.

(iv) There is also a linear strain coupling to octupole operators possible.[1,16] Again one can estimate the corresponding coupling constant only from PCM calculation, because the temperature dependence on the elastic constants is weak.[16] Again such contributions to the strain susceptibility based on PCM estimates can be neglected.[16] In summary we can say that, with the possible exception of B_6 terms, all other higher-order contributions should not effect our calculations seriously. We can state that our calculations should be correct within 10% and that the agreement with experiment is very good, considering the fact that we have no adjustable parameters.

There are three other points worth mentioning:

(i) In the frequency range 10–50 MHz we did not find any dispersion. In Fig. 2 we give results for 50 MHz and some points for 30 MHz. They show the same field dependence. For these low frequencies there should not be any dispersive effects.

(ii) The low-field behavior of the elastic constants is strictly quadratic. This we checked by separate measurements on an 14-kOe electromagnet. Both branches $[(k_z,R_x)$ and $(k_x,R_z)]$ show an H^2 dependence (Fig. 3) as expected.[10] At higher fields (where $g\mu H$ is no longer small compared to the CEF splittings) there are deviations from H^2 as shown in Fig. 2.

(iii) If one increases the temperature the magnetic field effect diminishes, because of the population of higher CEF states. This is also shown in Fig. 3 where the splitting between the two modes becomes smaller for $T = 4.3$ K.

C. TmSb: Rotational effects for the c_{11}-c_{12} mode

In Fig. 4 we show similar effects for the c_{11}-c_{12} mode, where we have plotted $\Delta v/v_0$ for the two modes $\vec{k} \parallel \vec{H}$ and $\vec{k} \perp \vec{H}$. As explained in Sec. II crystal TmSb (3) has two [110] and [1$\bar{1}$0] sides along which the magnetic field was aligned. Com-

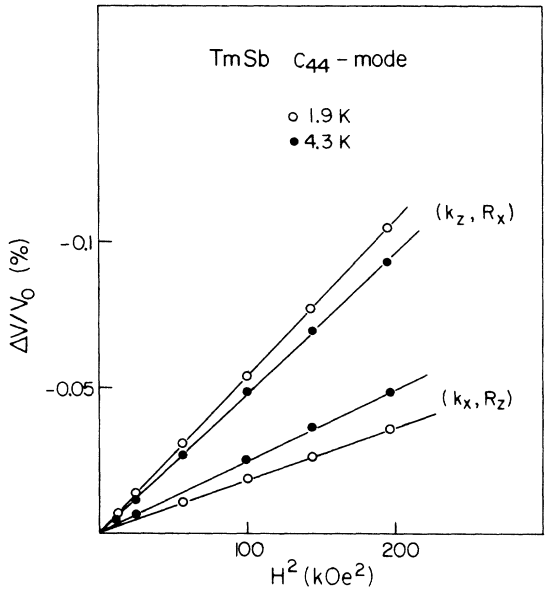

FIG. 3. Relative velocity change versus H^2 for small magnetic fields for the same c_{44} modes as in Fig. 2. Open circles, $T = 1.9$ K results; full circles, $T = 4.3$ K results.

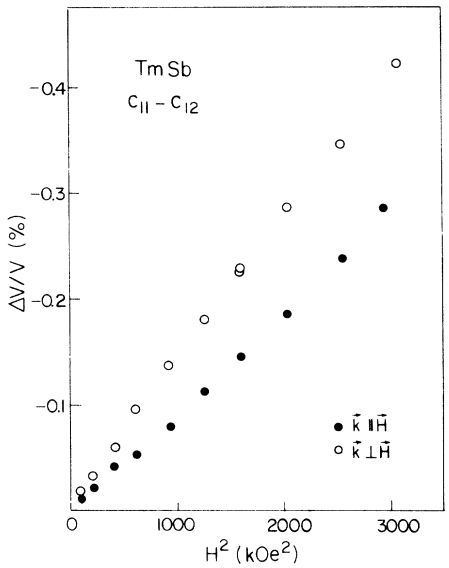

FIG. 4. Relative velocity change versus H^2 for large magnetic fields and for $c_{11}-c_{12}$ mode in TmSb for T = 2 K; full circles, $\vec{k}\|\vec{H}$, $\vec{R}\perp\vec{H}$; open circles, $\vec{k}\perp\vec{H}$, $\vec{R}\|\vec{H}$.

parison of Figs. 2 and 4 show that the effect for the c_{11}-c_{12} modes is smaller in absolute magnitude and also in the splitting of the two modes. Furthermore, in this case the $\vec{k}\|\vec{H}$ mode shows the smaller effect than the $\vec{k}\perp\vec{H}$ mode, opposite to what is observed in c_{44}. This is just a consequence of the different signs of G_2 and G_3.

For this mode we have to calculate CEF energy levels and wave functions for H along a [110] direction. This we did only for the truncated level scheme $\Gamma_1-\Gamma_4-\Gamma_5^2$. For the c_{44} mode such a calculation gives very similar results as if one uses the full CEF level scheme (see the Appendix). The neglect of, e.g., Γ_3 however, give drastic changes in the c_{11}-c_{12} strain susceptibility. Therefore, we only calculated terms from Eq. (5) which give rise to the splitting of the two c_{11}-c_{12} modes. We only state the difference between these modes $\Delta = (\Delta v/v)(\vec{k}\|\vec{H}) - (\Delta v/v)(\vec{k}\perp\vec{H})$. With this approximation we obtain for H = 40 kOe theoretically Δ = 0.0284%. This should be compared to the experimental value (Fig. 4) of Δ = 0.0825%. Although the discrepancy is about a factor of 3, the sign of Δ agrees with our expectation (opposite sign of G_2, G_3). We can state that also for the c_{11}-c_{12} mode the rotationally invariant magnetoelastic interaction gives the correct order of magnitude of the observed effect. A detailed quantitative analysis, involving the full CEF level scheme and possible higher-order interactions, might even improve the agreement between theory and experiment.

D. Pr_3Te_4

In Fig. 5 we show analogous measurements for the c_{44} mode for Pr_3Te_4 at T = 2 K and in low field. Rather large effects are observed in this case Δ = 0.024% for H = 14 kOe. The sign of the effect is opposite to the one for the c_{44} mode in TmSb. Pr_3Te_4 is not as well characterized as TmSb. The particular specimen measured did not show a magnetic phase transition down to 1 K, but the parameters indicate that it is an almost critically induced ferromagnet.[12] The CEF levels are only approximately known and because of the low point symmetry of the Pr^{3+} ion in this Th_3P_4 structure the wave functions are not known.[12] Therefore a quantitative analysis has to be postponed till more data are available on this compound.

E. Other substances

Similar effects have also been observed in $Pr_{0.05}La_{0.95}Al_2$ for the c_{44} mode in low field. Again we have to await experiments which determine the CEF levels before we can make a quantitative analysis.

SmSb would be another suitable substance to test rotationally invariant magnetoelastic effects because the material is well characterized[3] and the Sm^{3+} ($J=\frac{5}{2}$) ion splits in a cubic field into simple $\Gamma_7-\Gamma_8$ (65 K) states. This case with B_6 = 0 and this simple level scheme is therefore very favorable for a theoretical analysis,[10] although the existence of a magnetic phase transition with

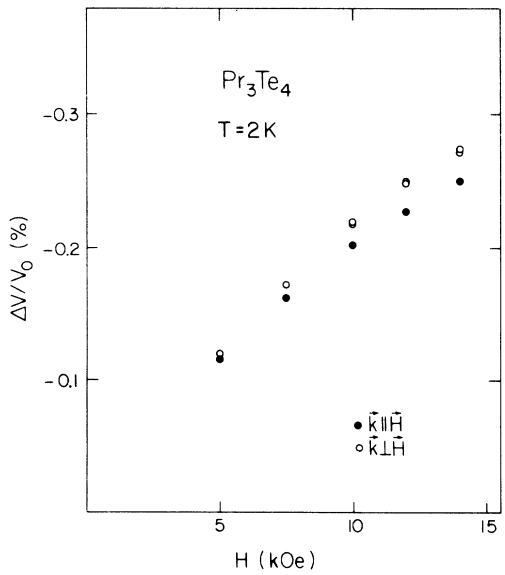

FIG. 5. Relative velocity change versus magnetic field for c_{44} mode in Pr_3Te_4 at T = 2 K; full circles, $\vec{k}\|\vec{H}$, $\vec{R}\perp\vec{H}$; open circles, $\vec{k}\perp\vec{H}$, $\vec{R}\|\vec{H}$.

TABLE I. Calculations for c_{44} for TmSb.

H (kOe)	0	20	40	60	80	Remarks
$\chi(\Lambda_{xz})$	−9069.1112	−9203.784	−9475.4408	−9754.3416	−10 007.5576	
$\chi(J_xJ_z)$	−25.492	−29.1364	−35.6844	−41.0784	−45.0568	
$\chi(J_xJ_z\Lambda_{xz})$	0	−12.5532	−40.7228	−73.6376	−108.1624	
$\langle\lambda_{xz}\rangle$	−84.0062	−83.9949	−83.8491	−83.5530	−83.1748	
$\langle J_x^2 - J_z^2\rangle$	0	−0.1778	−0.5235	−0.8384	−1.0842	
$\frac{\Delta v_{xz}}{v_0}$ (%)	0	−0.182	−0.5161	−0.8034	−1.0278	Full level scheme (Fig. 2)
$\frac{\Delta v_{zx}}{v_0}$ (%)	0	−0.1493	−0.4109	−0.6152	−0.7541	Full level scheme (Fig. 2)
$\frac{\Delta v_{xz}}{v_0}$ (%)	0	−0.1757	−0.4927	−0.7569	−0.9559	Only $\Gamma_1-\Gamma_4-\Gamma_5^2$ considered
$\frac{\Delta v_{zx}}{v_0}$ (%)	0	−0.1343	−0.3630	−0.5312	−0.6360	Only $\Gamma_1-\Gamma_4-\Gamma_5^2$ considered
$\frac{\Delta v_{zx}}{v_0}$ (%)	0	−0.1838	−0.5214	−0.8145	−1.0387	Full level scheme Inclusion of $\mathcal{H}^{(2)}$ contribution (Fig. 2)
$\frac{\Delta v_{xz}}{v}$ (%)	0	−0.1382	−0.4057	−0.6068	−0.7432	Full level scheme Inclusion of $\mathcal{H}^{(2)}$ contribution (Fig. 2)

$T_N = 2.11$ K could lead to additional effects for $T \geq T_N$. Unfortunately the quality of our crystal of SmSb was not good enough to warrant a successful investigation.

Apart from the cases studied so far and mentioned above (MnF_2, LVO_4, TmSb, Pr_3Te_4, $Pr_{0.05}La_{0.95}Al_2$, SmSb) there exist a calculation for rare-earth metals.[23] Due to the large magnetic moment, experiments for these systems are however difficult to interpret. The experimental corrections discussed above for TmSb (magnetostriction correction, demagnetizing field and its variation along the sound-wave path) are in this case very important and might mask the effect. In addition the material parameters are not known with sufficient accuracy to make a quantitative test.[24]

ACKNOWLEDGMENTS

We are very grateful to Professor E. Bucher for supplying us with the single crystals used in this research. We would like to acknowledge fruitful discussions with Dr. V. Dohm and Professor P. Fulde of the problems discussed in this paper.

APPENDIX

Here we give details of the calculation. In the case of the c_{44} mode with the external magnetic field H applied along the cubic [001] axis, we first calculated energies and wave functions for the CEF states. We used the tabulated wave functions[22] for $x = -0.8$ which is close to $x = -0.78$ calculated from CEF parameters.[21] With the Zeeman term $\mathcal{H}_z = -g\mu_B H J^z$ we diagonalized the Hamiltonian $\mathcal{H}_{\rm CEF} + \mathcal{H}_z$ and found new energies and wave functions. This we did for the full level scheme. Previously[11] we only took the lowest 3 levels $\Gamma_1 - \Gamma_4(25) - \Gamma_5^2$ (56 K). In the table we compare the differences between these two approaches. In the first 3 rows of Table I we list the contributions to the strain susceptibility (Eq. 7):

$$\chi[G_3(J_xJ_z + J_zJ_x) \pm 20B_4\Lambda_{xz}] = (20B_4)^2\chi(\Lambda_{xz}) + G_3^2\chi(J_xJ_z + J_zJ_x) \pm 40B_4G_3\chi(J_xJ_z + J_zJ_x)\Lambda_{xz} \quad \text{(A1)}$$

for selected magnetic field values and $T = 0$. The next two rows give the $T = 0$ values of $\langle\lambda_{xz}\rangle$ and $\langle J_x^2 - J_z^2\rangle$. Using Eq. (7) we give in the next 2 rows $\Delta v_{xz}/v_0$, $\Delta v_{zx}/v_0$. This we compare in the next two rows with $\Delta v/v_0$ values calculated only with the $\Gamma_1 - \Gamma_4 - \Gamma_5^2$ levels. One notes that the splitting of the 2 modes is actually increased by using the reduced level scheme by approximately 30%. These results are also shown in Fig. 2 for the full level scheme and in the Fig. of Ref. 11 for the truncated level scheme.

In the next 2 rows we give $\Delta v/v$ values with the effects of $\mathcal{H}^{(2)}$, Eq. (4) contributions included. This is also shown as the dotted line in Fig. 2.

†New address: Physikalisches Institut der Universität, Robert Mayerstr. 2-4, 6000 Frankfurt a. M., W. Germany.

*Work supported by NSF.

[1]E. R. Callen and H. B. Callen, Phys. Rev. 129, 578 (1963).

[2]E. R. Callen, J. Appl. Phys. 39, 519 (1968).

[3]B. Lüthi, M. E. Mullen, and E. Bucher, Phys. Rev. Lett. 31, 95 (1973); M. E. Mullen, B. Lüthi, P. S. Wang, E. Bucher, L. D. Longinotti, J. P. Maita, and H. R. Ott, Phys. Rev. B 10, 186 (1974).

[4]B. Lüthi, AIP Conf. Proc. 34, 7 (1976).

[5]H. F. Tiersten, J. Math. Phys. 5, 1298 (1964).

[6]W. F. Brown, Jr., J. Appl. Phys. 36, 994 (1965).

[7]R. L. Melcher, in *Proceedings of the International School of Physics, Enrico Fermi, Course LII*, edited by E. Burstein (Academic, London, 1972), p. 257.

[8]R. L. Melcher, Phys. Rev. Lett. 25, 1201 (1970).

[9]L. Bonsall and R. L. Melcher, Phys. Rev. B 14, 1128 (1976).

[10]V. Dohm and P. Fulde, Z. Phys. B 21, 369 (1975).

[11]P. S. Wang and B. Lüthi, Physica (to be published).

[12]E. Bucher, J. P. Maita, G. W. Hull, Jr., L. D. Longinotti, B. Lüthi, and P. S. Wang, Z. Phys. B 25, 41 (1976).

[13]E. Bucher, K. Andres, F. J. diSalvo, J. P. Maita, A. C. Gossard, A. S. Cooper, and G. W. Hull, Jr., Phys. Rev. B 11, 500 (1975).

[14]T. J. Moran and B. Lüthi, Phys. Rev. 187, 710 (1969).

[15]H. R. Ott and B. Lüthi, Phys. Rev. Lett. 36, 600 (1976).

[16]B. Lüthi, P. S. Wang, Y. H. Wong, H. R. Ott, and E. Bucher, Second International Conference on Crystal Field Effects in Metals and Alloys, Zurich, September, 1976 (Plenum, New York, to be published).

[17]The magnetoelastic coupling constants G_2G_3 in Eq. (1) are defined differently than in Ref. 3 (g_2,g_3). The relation is $G_2 = -\, g_2[(c_{11}-c_{12})6/N]^{1/2}$, $G_3 = -\, 2g_3\,(c_{44}/N)^{1/2}$.

[18]See, for example, M. T. Hutchings, in Solid State Physics, edited by F. Seitz and D. Turnbull (Academic, New York, 1964), Vol. 16, p. 227.

[19]V. Dohm, Z. Phys. B 23, 153 (1976).

[20]B. R. Cooper and O. Vogt, Phys. Rev. B 1, 1218 (1970).

[21]R. J. Birgeneau, E. Bucher, L. Passell, and K. C. Turberfield, Phys. Rev. B 4, 718 (1971).

[22]K. R. Lea, M. J. M. Leask, and W. P. Wolf, J. Phys. Chem. Solids 23, 1381 (1962).

[23]B. W. Southern and D. A. Goodings, Phys. Rev. B 7, 534 (1973).

[24]D. A. Goodings, Z. Phys. B 26, 37 (1977).